Proceedings of the {SEM} {XI} International Congress & Exposition on Experimental and Applied Mechanics. June 2-5, Orlando, FL USA 2008. Paper 136.

Impact generated stress waves and coupled fluid-structure responses

Kazuaki Inaba, Postdoctoral Scholar, Graduate Aeronautical Laboratories
Joseph E. Shepherd, Professor, Aeronautics and Mechanical Engineering
California Institute of Technology
1200 E. California Blvd, Pasadena, CA 91125, USA
joseph.e.shepherd@caltech.edu

ABSTRACT

We are studying strongly-coupled fluid-structure interaction generated by a stress wave propagating along the surface (as opposed to the usual case of normal incidence) in the fluid adjacent to a thin solid shell. This is realized experimentally through projectile impact along the axis of a water-filled tube. We have tested mild steel, aluminum (6061-T6), carbon-fiber (CFC), and glass-reinforced plastic (GRP) tubes 40 mm diameter and 0.8 mm wall thickness. A steel impactor is accelerated to 5–20 m/s using an air cannon and strikes an acrylic buffer or a polycarbonate buffer within the tube. Strain gages measure hoop and longitudinal strains every 100 mm. Elastic flexural waves are observed for impact speeds of 5–10 m/s and plastic waves appear for impact speeds approaching 20 m/s. Plastic flexural waves caused rupture of Al and CFC tubes at the closed end of specimen although the wave speeds were close to those predicted by the simple Korteweg theory.

1 Introduction

Impulsive loading and the resulting fluid-structure interaction has been extensively studied since WWII. The classical configuration of these experiments is a flat plate with loading created by the detonation of high explosives at some distance from the plate surface. Various combinations of depth, explosive charge size, plate materials and support methods have been used to examine the resulting motion and permanent deformation of the plate. For metal plates, the initial studies were carried out by Taylor 1941 and Kennard 1944, and subsequent work is reviewed by Nurick and Martin [1][2], Rajendran and Narashimhan [3]; for composites and laminates, recent work has been done by Despande and Fleck [4], Xue and Hutchinson [5]. The original analysis by Taylor identified a single dimensionless parameter Ψ that describes the coupling between the plate motion and fluid mechanics of the water. The coupling parameter is

$$\psi = \frac{\rho a \theta}{\rho_p h}$$

where ρa is the acoustic impedance of water, ρ_p is the mass density of the plate, h is the plate thickness and θ is the time scale for the blast wave decay. The peak plate velocity, maximum stress, and damage are functions of Ψ. Note that this coupling parameter involves not only the fluid and solid properties, but also the wave characteristic decay time so that the response is dependent on the particular model waveform that is used to create the loading.

Although the normal impact of an explosively generated shock wave on a plate is clearly extremely relevant to marine structure survivability, there are other aspects to fluid-solid coupling that are also important and much less studied. One of these is the coupling of flexural waves in plates and shells with the stress waves in a wave propagating perpendicular to the solid surface. To investigate this type of coupling, we are using projectile impact and thin-wall water-filled tubes to generate stress waves in the water that excite flexural waves in the tube wall, see Figure 1.

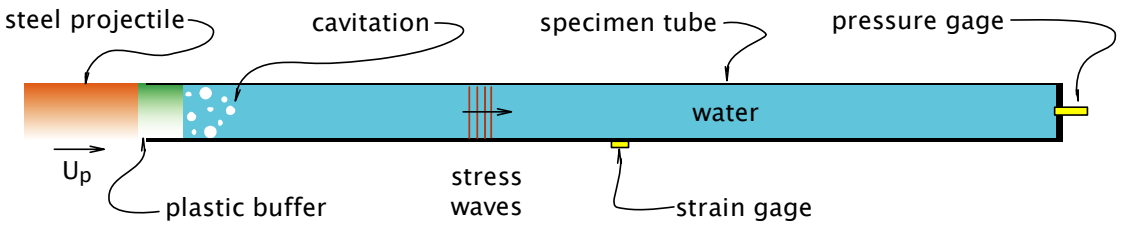

Figure 1 Schematic diagram of axi-symmetric water-in-tube configuration for generating flexural waves in a shell coupling with stress waves propagating in water.

This configuration is similar to that used by Trevena [6] and more recently by Skews et al [7], and independently proposed as an underwater shock simulator by Despande et al [4]. With a piston velocity of 250 m/s, it is possible to create peak shock pressures of 480 MPa if the tube is considered to be rigid. The actual shock pressure may be significantly lower, depending on the extent of fluid-solid coupling for this configuration. The problem of stress waves propagating in a water-filled tube have been considered extensively in the context of water hammer beginning with Korteweg (1878), Joukowsky (1898), and recently reviewed by Skalak [8] and Tijsseling [9]. There are four axisymmetric modes of deformation for low-amplitude waves (Fuller and Fahy [10], Shinha et al [11], Pinnington [12]) and the most significant of these for the present study is the Korteweg mode which is a radial oscillation of the tube coupled to longitudinal motion of the liquid. The extent of fluid-solid coupling in this geometry is determined by a different parameter.

$$\beta = \frac{K}{E}\frac{D}{h}$$

Where K is the fluid bulk modulus, E is the solid Young's modulus, D is the tube diameter, and h is the wall thickness. In this case, the coupling is independent of the blast wave characteristics and only depends on the fluid and solid properties and geometry. The Korteweg waves travel at a speed (Lighthill [13])

$$c = \frac{a_f}{\sqrt{1+\beta}}$$

which, depending on the magnitude of β, can be significantly less than the sound speed a_f in the fluid or the bar wave speed $\sqrt{E/\rho_s}$ in the tube. In the current experiments, parameter β is sufficiently large (1.5 for the aluminum tubes) that we anticipate significant fluid-solid coupling effects. Previous experiments in our laboratory (Shepherd [14]) on flexural waves excited by gaseous detonation are superficially similar to the present study but these have all been in the regime of small β.

2 Experimental setup

The current facility is a low speed gas gun that is mounted vertically above a specimen tube filled with water. The 0.67 kg steel projectile is accelerated by a combination of gravity and compressed air using driver (reservoir) pressures between 0.14 and 0.68 MPa above ambient. The projectile fits closely into the barrel and is lubricated with WD-40 before each test. Prior to installing the specimen tube, the projectile is loaded into the barrel and using a vacuum pump, the projectile is sucked up to the top and held against a rubber seal by the pressure of the air in the barrel. After the specimen tube is aligned and the instrumentation is connected, the projectile is launched down to the tube. The air reservoir is filled to the desired pressure, the vacuum line is closed, and a remotely-operated valve connects the air reservoir to the evacuated region above the projectile.

The projectile is not completely ejected from the barrel when it impacts an acrylic or polycarbonate buffer placed on the water surface which is just inside the specimen. In this fashion, the stress waves due to the impact of the projectile are transmitted to the water inside the specimen tube. This prevents the projectile from impacting the specimen tube directly and since the projectile does not completely emerge from the barrel, it eventually rebounds back inside the barrel without damaging the end of the barrel.

The impact generated stress waves in the water cause the tube to deform and the resulting coupled fluid-solid motion propagates down the tube. The deformation of the tube is measured by strain gages oriented in the hoop and longitudinal directions and the pressure in the water is measured by a piezoelectric transducer mounted in an aluminum fitting glued to the bottom of the tube. The bottom of the tube was mounted in a lathe chuck that was placed directly on the floor.

In our tests, four types of tube specimens were examined. Shots 8-13 were carried out using seamless aluminum tubing of AL6061-T6 specification. The tubes had a nominal wall thickness of 0.86 mm, inner diameter of 39 mm, and were about 0.9 m long. Shots 14-16, 40-51, 57, 58 were carried out with carbon-fiber composite (CFC) tubes (1.45 mm thickness wall, 38.2 mm inner diameter, 0.9 m long, type GR-CFRWT manufactured by Graphtek LLC and Black Project™ Carbon Fiber Tube) which consisted of a longitudinal fiber core with a woven cloth over-wrap and vinylester resin. Shots 17-21, 28, 29, 30-35 were conducted with mild steel tubes (0.77 mm thickness, 40.0 mm inner diameter, 0.9 m long). Detailed results of experiments with mild steel tubes are discussed in a separate paper [15]. Finally, Shots 36-39 were performed with a fiberglass-reinforced plastic (GRP) tube (1.60 mm thickness, 38.8 mm inner diameter, 0.9 m long) with a winding angle of 40 degrees (Airframe Tubes by Hawk Mountain Enterprises).

Each test specimen is instrumented with 14 strain gauges for measuring hoop and longitudinal strains. A

single piezoelectric pressure transducer recorded the pressure wave reflected from the aluminum plug at the bottom of the specimen. A high-speed video camera (Vision Research Phantom 5) is used to observe the impact against the buffer and distance-time measurements taken directly from the images were used to determine the speed of the projectile immediately prior to impact.

The projectile speed at the exit of the barrel was varied by using different pressures in the gas reservoir. Although there is substantial variability in the exit speed, there is a clear trend of increased projectile speed with increasing reservoir pressure. The projectile exit speed is about 5 m/s without driver gas and with increasing driver pressure, the speed is between 6 and 20 m/s at barrel exit. Variations in friction, seating of the projectile against the rubber seal, low accuracy of the projectile speed measurement system, and the timing of the filling and discharge process all contributed to the variability in the gun performance. The buffer speed immediately after the projectile impact is extracted from the movies. It is confirmed that the maximum buffer speeds are 2-3 m/s lower than the projectile impact speeds [15].

3 Results and discussion

The impact of the steel projectile on the water results in a deformation (strain) wave in the surrounding tube with a well-defined front propagating at a nearly constant speed. The reverberation of the impact-generated stress waves within the steel projectile and plastic buffer results in a decaying pressure (and strain) behind the initial front. The strain and pressure histories measured in the experiments reveal that additional coupled pressure and strain waves are created by wave reflection processes when the waves reach the tube ends, and that waves are generated if the tube ruptures.

Tests using a driver pressure of 0.14 MPa result in impact velocities of less than 10 m/s, causing elastic strain waves in Al, CFC, MS, and GRP tubes. The peak strains at 0.14 MPa driver pressures are close to or less than 0.2%. Plastic strain waves are created by increasing the driver pressure. Peak strains at 0.64 MPa driver pressures are close to 0.4% for Al tubes, 0.6-0.7% for CFC tubes, 0.3% for MS tubes, and more than 0.7% for GRP tube. The values of the peak plastic strains gradually decrease as the wave moves from the impact point toward the bottom while the peak elastic strains appear to be independent of the wave position. Similar results were obtained in the case of gaseous detonation-excited flexural waves (Beltman et al [16], Beltman and Shepherd [17]). The flexural waves excited by gaseous detonations are oscillatory and damp very slowly.

Figure 2 shows hoop strain histories measured by strain gages located at 100 mm intervals (lower seven traces in the figures) and pressure history at the bottom of the specimen (top trace in the figures). The traces are displaced by an amount proportional to the difference in spatial location of the gages so that wave propagation processes can be clearly identified. The strain wave front speeds are 930 and 864 m/s. Strain waves observed in the Al tube are distinct and reflections from the bottom and the top boundaries are readily observed. Strain waves in the CFC tube (Figure 3) show a more complex behavior than those in the Al tube due to the anisotropic nature of the material with differing properties in the longitudinal and hoop directions.

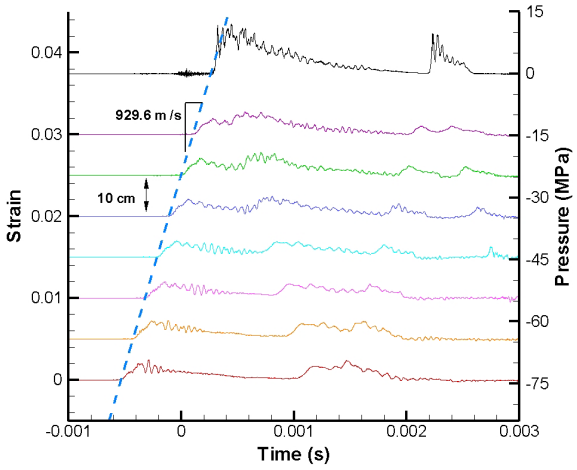

Figure 2 Hoop strain histories and pressure history in Shot 11. Aluminum tube, 8.9 m/s impact speed.

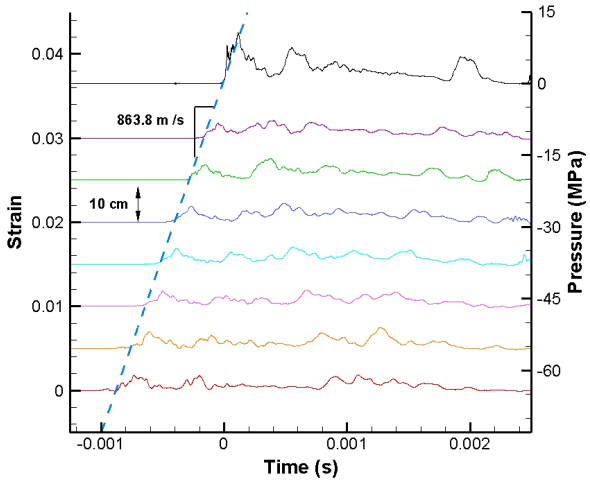

Figure 3 Hoop strain histories and pressure history in Shot 15. CFC tube, impact speed 7.7 m/s.

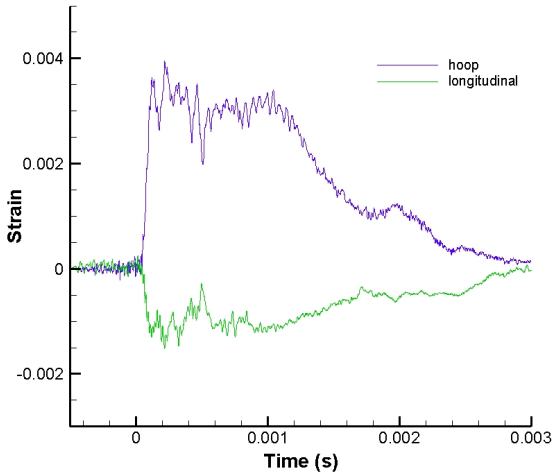

Figure 4 Hoop and longitudinal strain histories located at the same distance from the tube top in Shot 13. Al tube, impact speed 17.0 m/s.

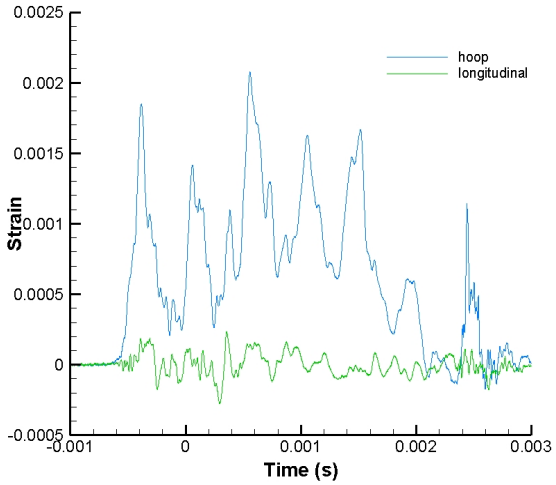

Figure 5 Hoop and longitudinal strain histories in Shot 15. CFC tube, impact speed 7.7 m/s.

Longitudinal and hoop stress are compared at one location for the Al (Figure 4) and CFC (Figure 5) specimens. For the Al tube, the longitudinal and hoop strains are strongly correlated and positive strains in the hoop direction result in negative longitudinal strain. The sign and the magnitude (longitudinal strain is about -1/3 of the hoop strain) is the expected result based on the Poisson effect for an isotropic material. For the CFC tube, the longitudinal strain is a much smaller fraction of the hoop strain (1/10) than for the aluminum tubes and shows an effective negative Poisson effect with positive hoop strain being correlated with positive longitudinal strain.

Tests using a driver pressure of 0.64 MPa result in impact velocities of 19 m/s and create plastic strain waves in the aluminum tubes. The wave front rise time is faster for the plastic waves than the elastic waves and the subsequent reflections are less well defined for plastic than elastic cases. The wave front speed derived from Figure 6 is 946 m/s, slightly higher than for the elastic cases.

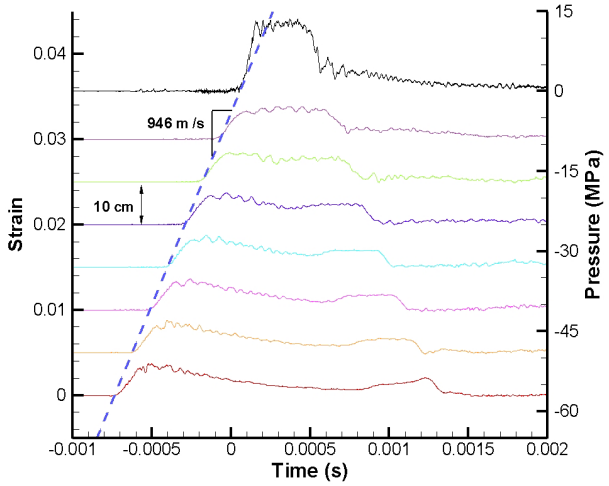

Figure 6 Hoop strain histories and pressure history in Shot 10. Al tube, impact speed 15.8 m/s, tube rupture.

The tubes ruptured in Shots 10 and 16. The loss of pressurization limits the peak pressure and results in an expansion wave being created. This can be observed in the strain and hoop histories of Figure 6 and Figure 7. The tube rupture is indicated by a sudden pressure decrease at 0.5 ms which then propagates back up the tube as indicated by the arrival of the relaxation wave front in the strain signals. Rupture in the CFC tube is much more dramatic than in aluminum since the failure in CFC is by a high-speed brittle fracture rather than the ductile rupture that is observed in the aluminum tubes. Rupture of the CFC tube occurred on the first high impact speed test while the ductility of the aluminum tube delayed rupture until the damage had accumulated from a number of successive impacts. The Al tube used in Shot 10 experienced 9 impacts before the rupture shown in Figure 8 was created. The same type of crack is observed in the process of gaseous detonation propagation within similar tubes (Chao and Shepherd [18]), although previous studies on fracture used deliberate flaws to initiate fracture. In the present case, the pressure is sufficiently high that the stress concentrations associated with the imperfectly cut end of the tube appear to have initiated the fracture process.

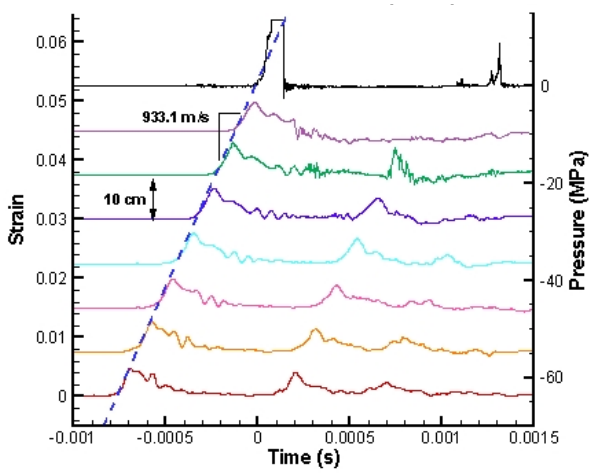

Figure 7 Hoop strain histories and pressure history in Shot 16. CFC tube, impact speed 16.5 m/s, tube rupture.

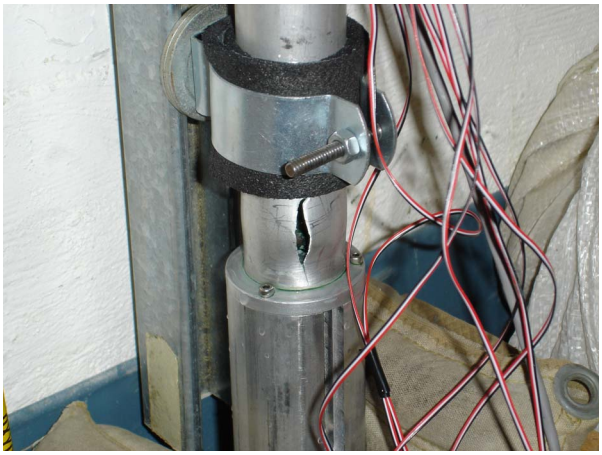

Figure 8 Tube rupture in Shot 10. Al tube, impact speed 15.8 m/s, 50 mm rupture length.

The CFC tube rupture was in the form of a long, straight crack parallel to the tube axis and serendipitously intersected the longitudinal strain gages so that the strain signals can be used to deduce the apparent crack tip speed to be about 2000 m/s, These are much higher than typical crack tip speeds of 200-300 m/s observed (Chao and Shepherd [18], Chao and Shepherd [19]) in detonation-driven fracture of aluminum. However, this value is actually quite a bit lower than crack tip velocities of up to 7000 m/s that were observed by Coker and Rosakis [20] in impact experiments on mode I and II cracks in unidirectional graphite-epoxy composite plates. As discussed in Chao and Shepherd, the cracks in internally-pressurized tubes initiate in Mode I since the major principal stress is in the hoop direction, perpendicular to the initial crack tip motion. However, in thin ductile tubes, the plastic deformation of the material adjacent to the crack quickly results in a transition to mixed mode fracture.

At the reflected boundary, the CFC tubes always burst for the tests with higher driver pressures while a GRP tube remained intact under these same conditions. Shot 37 and 39 were conducted with the GRP tube at projectile impact speeds of 6.8 m/s and 18.8 m/s, respectively. Figure 9 and Figure 10 show hoop and longitudinal strain histories in Shot 37. Hoop strains are similar to the profiles of the CFC tubes. In contrast to the CFC tubes, the GRP tube indicated a longitudinal strain history similar to that observed in the Al tubes. Longitudinal strains have more correlation to hoop strains than those with the CFC tubes, though the hoop-longitudinal coupling is clearly more complex that in Al. Primary wave velocities measured for the hoop and longitudinal wave fronts are 904 m/s and 899 m/s, similar to those of the CFC tubes. In Shot 39, frontal peaks of hoop strains become larger than 0.7% but residual strain on the reflected boundary is still negligible after the experiment. Hoop and longitudinal strain histories of Shot 39 are given in Figure 11 and Figure 12. The primary flexural wave velocities are 949 m/s and 916 m/s, slightly faster than those in Shot 37.

Skalak [8] proposed that there are two types of dominant flexural waves with different phase velocities; the precursor wave (faster and smaller deflection) and the primary wave (slower and larger deflection). Although the primary hoop strain is about 3-4 times larger than the primary longitudinal strain, the precursor longitudinal strain is 10 times larger than the precursor hoop strain. For this reason, the precursor longitudinal wave is clearly observed but the precursor hoop strain is not. In order to observe the differences in the two cases, the axis range in Shot 39 is set to be three times larger than in Shot 37 and the axis range of hoop strain is double of the range of the longitudinal strains. In comparison with Shot 37, the hoop strains in Shot 39 show steeper spikes at the primary wave front. Longitudinal strains in Shot 39, however, show fewer fluctuations and stronger correlations to the hoop strain than in Shot 37. Moreover, precursor longitudinal strains are clearer in Shot 39 than in Shot 37. Similar features in the longitudinal strains are observed with steel tubes [15]. Most of the fibers in the CFC tube are running in the longitudinal direction, which results in a much higher longitudinal than hoop modulus. In the GRP tube, fibers run at a shallow angle to the circumferential direction, making the tube much stiffer (and stronger) in the hoop direction than the CFC tubes.

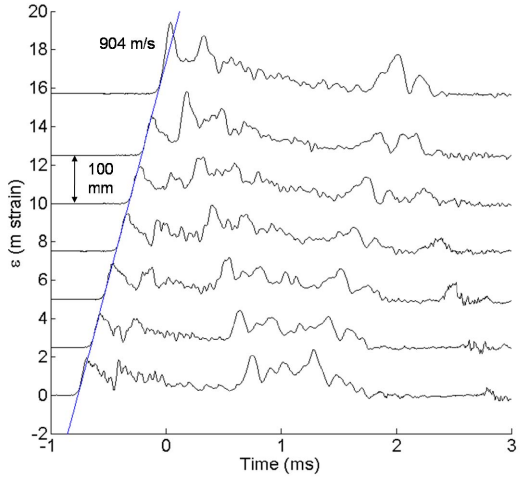

Figure 9 Hoop strain histories in Shot 37. GRP tube, impact speed 6.8 m/s.

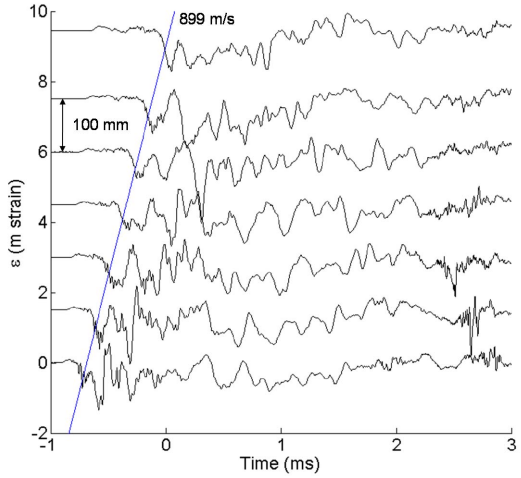

Figure 10 Longitudinal strain histories in Shot 37. GRP tube, impact speed 6.8 m/s.

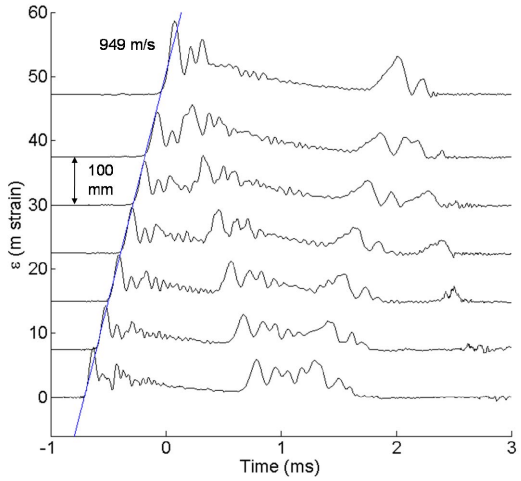

Figure 11 Hoop strain histories in Shot 39. GRP tube, impact speed 18.8 m/s.

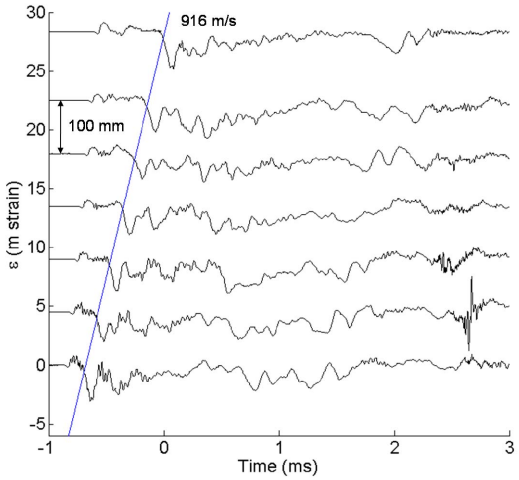

Figure 12 Longitudinal strain histories in Shot 39. GRP tube, impact speed 18.8 m/s.

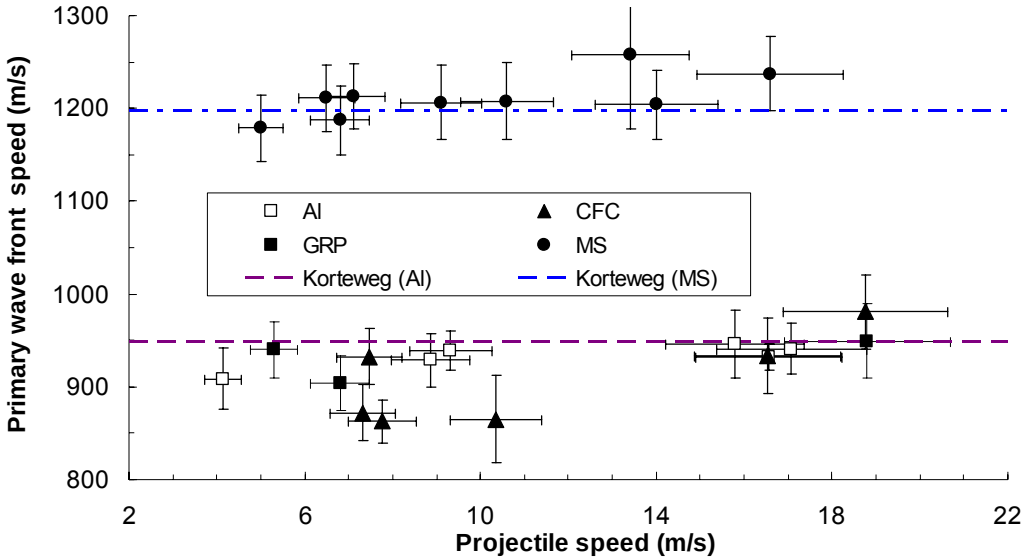

Figure 13 Relation between stress wave front speed and projectile speed. Al and mild steel (MS) wave velocities are also derived from the Korteweg theory.

Measured stress wave velocities as a function of projectile velocities are summarized in Figure 13. The most striking result is that the flexural waves propagate much slower than either the sound speed in water (1500 m/s) or tube bar speeds (Al 5100 m/s, CFC 9500 m/s, MS 5200 m/s, GRP 5300 m/s). This is due to the flexural motion in tube being strongly coupled to compression wave in water. The predicted velocities with the simple Korteweg theory are 950 m/s for Al and 1200 m/s for mild steel and correlate well with the experimental results. There appears to be a trend of increasing wave speed with impact velocity but there is a substantial amount of scatter and it would be premature to draw any conclusions about the dependence of wave speed on amplitude. We know of no theoretical treatment for the Korteweg wave speed in general composite materials although Pinnington [12] treats the related problems of a wire reinforced hose. Based on the experimentally measured

wave front speed of about 900 m/s for elastic flexural waves in CFC and GRP tubes, the effective coupling parameter β can be computed using the simple Korteweg model to be about 1.81 and 1.75, respectively. The tensile modulus of the carbon epoxy composite (CFC) is typically 140 GPa along the fiber direction while effective modulus derived from the present tests is 33 GPa. This is consistent with a relatively low Young's modulus in the hoop direction of the CFC material which is to be expected since the majority of the carbon fibers are aligned in the longitudinal direction. According to Watters [21], elasticity modulus for common GRP pipe is 27.6 GPa and is close to the effective Young's modulus derived from the present tests with the GRP tube (32 GPa).

4 Conclusion

We used projectile impact and aluminum, carbon-fiber composite, mild steel, and glass-reinforced plastic tubes filled with water to study the propagation of coupled structural and pressure waves. Tests using a driver pressure of 0.14 MPa resulted in impact velocities of less than 10 m/s, creating elastic strain waves. The peak strains at 0.14 MPa driver pressures were close to or less than 0.2%. Plastic strain waves were created by increasing the driver pressure. The strain and pressure histories measured in the experiments revealed that additional coupled pressure and strain waves are created by wave reflection processes when the waves reach the tube ends, and that waves are generated if the tube ruptures. Hoop and longitudinal strains measured in composite tubes strongly depended on the fiber direction. Flexural waves in tube coupled to compression wave in water propagated in the water hammer mode and much slower than either the sound speed in water or tube bar speed.

Acknowledgements

This research was sponsored by the Office of Naval Research, DOD MURI on Mechanics and Mechanisms of Impulse Loading, Damage and Failure of Marine Structures and Materials (ONR Grant No. N00014-06-1-0730), program manager Dr. Y. D. S. Rajapakse. We thank Chris Krok for his work on the first generation of experiments and Tim Curran for his work on data processing and image analysis.

References

[1] Nurick GN, Martin JB. Deformation of thin plates subjected to impulsive loading—a review, Part II: experimental studies. Int J Impact Eng 1989;8(2):171–86.

[2] Nurick GN, Martin JB. Deformation of thin plates subjected to impulsive loading—a review, Part I: theoretical consideration. Int J Impact Eng 1989;8(2):151–70.

[3] R. Rajendran and K. Narasimhan. Deformation and fracture behaviour of plate specimens subjected to underwater explosion - a review. International Journal of Impact Engineering, 32:1945–1963, 2006.

[4] V. S. Deshpande, A. Heaver, and N. A. Fleck. An underwater shock simulator. Proc. R. Soc. A, 462: 1021–1041, 2006.

[5] Z. Xue and J. W. Hutchinson. A comparative study of impulse-resistant metal sandwich plates. International Journal of Impact Engineering, 30:1283–1305, 2004.

[6] D.H. Trevena. Cavitation and Tension in Liquids. Adam Hilger, 1987.

[7] B.W. Skews, E. Kosing, and R.J. Hattingh. Use of a liquid shock tube as a device for the study of material deformation under impulsive loading conditions. Proc. Instn. Mech. Engrs. J. Mechanical Engineering Science, 218:39–51, 2004.

[8] R. Skalak. An extension to the theory of water hammer. Transactions of the ASME, pages 105–116, January 1956.

[9] A.S. Tijsseling. Fluid-structure interaction in liquid-filled pipe systems: A review. Journal of Fluids and Structures, 10:109–146, 1996.

[10] C. R. Fuller and F. J. Fahy. Characteristics of wave propagation and energy distributions in cylindrical elastic shells filled with fluid. J. Sound Vibration, pages 501–518, 1982.

[11] B. K. Sinha, T. J. Plona, S. Kostek, and S.-K. Chang. Axisymmetric wave propagation in fluid-loaded cylindrical shells. J. Acoust. Soc. Am., 92, August 1992.

[12] R. J. Pinnington. The axisymmetric wave transmission properties of pressurized flexible tubes. Journal of Sound and Vibration, 204:271–289, 1997.

[13] J. Lighthill. Waves in Fluids. Cambridge University Press, 1978.

[14] J. E. Shepherd. Structural response of piping to internal gas detonation. In ASME Pressure Vessels and Piping Conference. ASME, 2006. PVP2006-ICPVT11-93670, July 23-27 2006 Vancouver BC Canada.

[15] K. Inaba and J.E. Shepherd. Flexural waves in fluid-filled tubes subjected to axial impact. In ASME Pressure Vessels and Piping Conference. ASME, 2008. PVP 2008-61672, July 27-31 2008 Chicago IL USA.

[16] W.M. Beltman, E. Burcsu, J.E. Shepherd, and L. Zuhal. The structural response of cylindrical shells to internal shock loading. Journal of Pressure Vessel Technology, pages 315–322, 1999.

[17] W.M. Beltman and J.E. Shepherd. Linear elastic response of tubes to internal detonation loading. Journal of Sound and Vibration, 252(4):617–655, 2002.

[18] T.-W. Chao and J. E. Shepherd. Comparison of fracture response of preflawed tubes under internal static and detonation loading. Journal of Pressure Vessel Technology, 126(3):345–353, August 2004.

[19] T.-W. Chao and J. E. Shepherd. Fracture response of externally flawed aluminum cylindrical shells under internal gaseous detonation loading. International Journal of Fracture, 134(1):59–90, July 2005.

[20] D. Coker, A. J. Rosakis. Experimental observations of intersonic crack growth in asymmetrically loaded unidirectional composite plates. Philosophical Magazine A-Physics Of Condensed Matter Structure Defects And Mechanical Properties 81 (3): 571-595 Mar 2001.

[21] G.Z. Watters. Analysis and Control of Unsteady Flow in Pipelines. Butterworths Publishers, 1984.